

High-Pulsed Electromagnetic Field Generator for Contactless Permeabilization of Cells *In Vitro*

V. Novickij¹, M. Kranjc², G. Staigvila¹, J. Dermol-Černe², J. Meleško³, J. Novickij¹, and D. Miklavčič²

¹Faculty of Electronics, Vilnius Gediminas Technical University, 03227 Vilnius, Lithuania

²Faculty of Electrical Engineering, University of Ljubljana, 1000 Ljubljana, Slovenia

³Faculty of Fundamental Sciences, Vilnius Gediminas Technical University, 03227 Vilnius, Lithuania

High-intensity pulsed electromagnetic fields (HI-PEMFs) can be used for contactless permeabilization of biological cells and, thus, exploited for drug and gene delivery or other biomedical applications. Nevertheless, the availability of applicable technological setups is almost non-existent. In this article, we present a new prototype of the HI-PEMF generator, which can be used for contactless permeabilization of cells *in vitro*. The generator is based on high dl/dt silicon controlled rectifier (SCR) switches and is capable to generate magnetic field pulses up to 7 T and electric fields >10 V/cm in a volume comparable to standard *in vitro* procedures for electroporation. Three different applicators (inductors) were studied, and the influence on the output pulse is presented, including the thermal analysis. Based on the results, the optimal inductor was selected and experimentally tested on Chinese hamster ovary (CHO) cells in basic permeabilization [propidium iodide (PI)] experiments. The generator circuit, parameters, characteristics, and recommendations for future HI-PEMF systems are provided.

Index Terms—Biological interactions, biomembranes, cells, electromagnetic fields, pulsed power systems.

I. INTRODUCTION

THE capability to increase the permeability of the cell membrane for initially impermeable molecules opens an opportunity for numerous biomedical and biotechnological applications. As a result, one of the most successful and widely established permeabilization methods (including clinics) is based on electroporation, which is a phenomenon of controlled permeabilization of the cell membrane by pulsed electric fields (PEFs) [1]–[3]. Electroporation has found high applicability in the area of cancer treatment as a tissue ablation (irreversible electroporation) [4], [5] or drug delivery (reversible electroporation) methodology [6]. Due to the physical nature of the process and the variety of triggered effects, the area of its application is constantly expanding [7]–[9].

Technology-wise PEF treatments employ pulsed power setups to generate ns–ms range electrical pulses in the range from several hundreds of volts to tens of kilovolts [10]–[12], while a square wave waveform is the most common nowadays (both unipolar [13] and bipolar pulses are used [14], [15]). Sinusoidal pulses were also shown to achieve electroporation [6]. Nevertheless, electroporation-based treatments have some limitations. Taken that the effectiveness depends on the pulse amplitude, duration, number of pulses, frequency, and other factors [16]–[20], the experimental flexibility is already quite high, and comparison of the procedures is not always straightforward [21], [22]. On the other hand, the multifactorial flexibility opens the capabilities for designing precise and case-specific procedure. However, most of the struggle is in the area of PEF applicators. As an applicator, various types of

electrodes are used [23]–[26], while for deep-seated tumors invasive electrodes are applied and, thus, increase treatment planning time and risks [27], [28].

First, the distribution of the electric field is non-homogeneous due to various conductivity gradients present in tissues [29], [30]. As a result, complex and time-consuming treatment planning is required for each individual case, but still the outcome (i.e., pulse forming and resultant PEF distribution) are predicted only with a certain degree of accuracy rather than guaranteed [31]. Second, the high-voltage electrical pulses trigger severe muscle contractions [32], which depending on the tumor localization may require additional anesthetic management [33] or synchronization with electrocardiography signal in case of treatments close to the heart [34]. In addition, electrochemical reactions [35], [36] in the vicinity of the electrodes may involve deviation in the tumor response, alter drug chemotherapeutic activity, or induce pH damage due to the release of metal ions and altered pH [37]–[39]. Finally, the requirement of good contact between the electrodes and tissue must be highlighted [40] as one of the disadvantages, since it affects both the distribution of PEF, the current density [41], and risks of voltage breakdown [42]. Therefore, contactless or at least non-invasive approaches would be welcomed.

One of the promising concepts to address the problem is the application of high-intensity pulsed electromagnetic field (HI-PEMF) that can be delivered using contactless applicators. Proof of concept was first introduced in 2012 [43], [44] and is based on high dB/dt pulses, which induce PEMF sufficient to trigger cell permeabilization. Surprisingly, the induced electric field in HI-PEMF is by several orders of magnitude lower than the minimal threshold field in conventional electroporation [45]. Currently, it is known that both the electric and magnetic field (MF) components are playing a role during HI-PEMF permeabilization [46]; however, the exact mechanism of action is not yet established. Nevertheless, the

Manuscript received December 5, 2019; accepted February 28, 2020. Date of publication March 6, 2020; date of current version April 17, 2020. Corresponding author: V. Novickij (e-mail: vitalij.novickij@vgtu.lt).

Color versions of one or more of the figures in this article are available online at <http://ieeexplore.ieee.org>.

Digital Object Identifier 10.1109/TMAG.2020.2979120

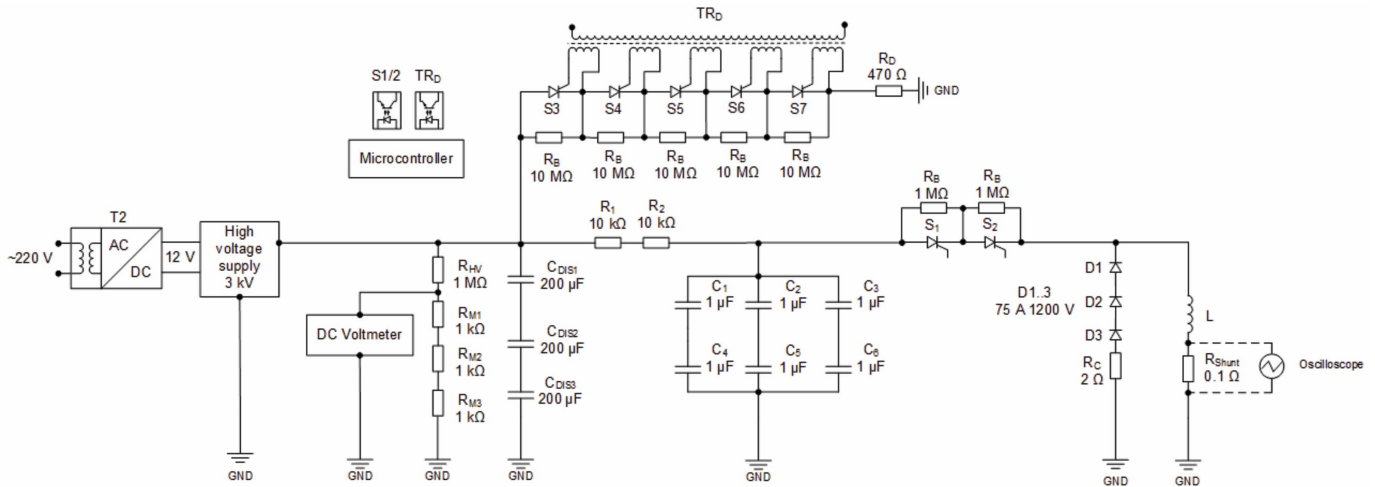


Fig. 1. Principal circuit of the pulsed electromagnetic field generator.

in vivo effectiveness of contactless HI-PEMF is comparable to conventional PEF procedure [43], [45], [47]. The *in vitro* permeabilization is harder to achieve, but still the proof of concept was presented [44], [48]–[50].

In order to continue the development of the methodology further, a parametric study of the PEMF effects is required; however, the availability of applicable pulsed power setups is almost non-existent primarily due to the high demanding current and voltage handling parameters. For example, a typical *in vitro* system must support currents in kiloampere range and high di/dt [51], [52], which is already a challenge with inductive load. The management of the Joule heating [50], [53] and transients further introduce complexity in system design, which is considerably higher compared to conventional electroporation setups.

During the past 5 years, several *in vitro* HI-PEMF prototypes were introduced [51], [54]–[57]. However, the tradeoff between the effective treatment volume and the peak parameters had to be established. For example, the generator presented in 2013 was operated with a volume of $3 \mu\text{L}$ [55], and an improved 5.5 T version was capable of handling $20 \mu\text{L}$ [50]. Nevertheless, when the parameters are reviewed in the context of Joule heating (more than 10°C even with cooling), the versatility of the setup is diminished. Several other low volume setups based on MOSFETs [56] and IGBTs [51] were also considered; however, in the end, the applicability was limited to object-specific experiments due to Joule heating and low volume of the sample. In the case of higher volume systems, an ignitron-based prototype was proposed recently, which is promising [58]. However, as a tradeoff, the pulse shape is more an oscillation rather than a pulse, which also can be regarded as a limitation.

Therefore, in this article, we present a tradeoff and, currently, an optimal system for HI-PEMF experiments *in vitro*, which was developed based on past experience.

II. PULSE GENERATOR

A. Parameters of the Setup

In order to establish parameters for the new generator, available knowledge on HI-PEMF methodology was analyzed. It is known that the high dB/dt systems are preferable due

to highly induced electric field, as apparently amplitudes in the range of 2–3 T and 2–5 V/cm are already sufficient to trigger cell membrane permeabilization [44], [45]. However, when cuvette-like containers are used, *in vitro* 3 T, 7.2 V/cm treatment barely triggers any permeabilization in mammalian cells [49]. Increasing the electric component to 100–175 V/cm and application of bipolar pulses (without an increase of the MF amplitude) improves the permeabilization rate, but not radically [59]. Nevertheless, permeabilization without the PEF component is not possible [46], which implies that at least 5 V/cm induced electric field should be ensured in the new setup. The highest (currently reported) *in vitro* permeabilization efficiency was achieved when unipolar microsecond range of 5.5 T pulse was used (7–8 V/cm); however, the Joule heating ($>10^\circ\text{C}$) and small sample volume ($20 \mu\text{L}$) were a limitation [50]. Therefore, in this article, we have decided to double the induced electric field to be $>15 \text{ V/cm}$, increase the effective volume to be at least $40 \mu\text{L}$, and keep the MF in the 5–7 T range while minimizing the influence of Joule heating.

B. Development of the Pulse Generator

In order to ensure the parameters described above, an improved topology of the generator reported in [50] and [55] was developed. Previously, the generator supported current up to 550 A, thus taken into account the requirement to double the volume, while maintaining a comparable pulse amplitude, the current handling should be in the range of 1.2–1.5 kA. For this purpose, two MCC255-16io1 (IXYS, Milpitas, CA, USA) silicon-controlled rectifier (SCR) modules S1 and S2 were used in series (see Fig. 1). Such configuration supports current handling up to 10 kA and voltage handling up to 3.2 kV. Nevertheless, using currents higher than 1.5 kA will be disadvantageous from the perspective of Joule heating. Also, SCRs are limited by di/dt (in this case $500 \text{ A}/\mu\text{s}$); therefore, taken that we were aiming for high dB/dt pulse, the SCR will be performed on its limit already. The power circuit included two capacitor batteries: 1) for filter-type capacitor (KNG1914, ISKRA, Ljubljana, Slovenia) purposes ($3 \mu\text{F} \times 200 \mu\text{F}$ in series = $66.67 \mu\text{F}$) and 2) for high di/dt pulse forming (940C20W1K-F, Cornell Dubilier, Calexico, CA, USA; $6 \mu\text{F} \times 1 \mu\text{F}$ in series and parallel = $1.5 \mu\text{F}$).

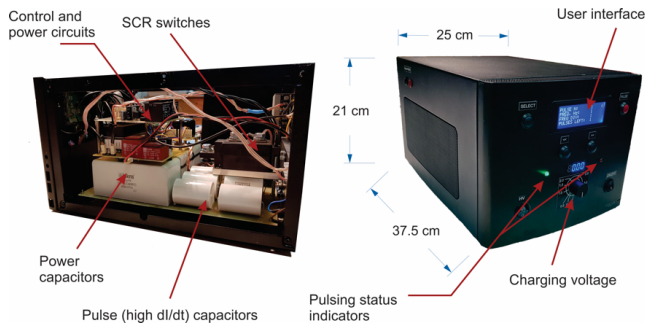


Fig. 2. Developed HI-PEMF generator, inside of the generator (left) and housing of the generator (right).

The capacitors were charged (0–3 kV) using an UM4*4 (Spellman, Hauppauge, NY, USA) voltage converter. A series resistance of 20 k Ω was introduced between the capacitor batteries to support repetitive pulsing (up to 5 Hz). Crowbar circuit (D1–3, R_C) was used to form unipolar pulse without the influence of reverse voltage and to minimize the reverse charge of the capacitors. As a load, any type of inductor can be used with a recommended value of $5 + \mu\text{H}$, which will ensure 1 + kA range current and rise/fall times within the limits of selected SCRs. For safety reasons, an emergency discharge circuit (S3–S7) was implemented. It is triggered by a galvanically decoupled trigger (TR_D), which is separated from the main microcontroller (XMEGA128, Atmel, San Jose, CA, USA). The developed HI-PEMF generator is shown in Fig. 2.

As shown in Fig. 2, the generator is compact and features the size of $25 \times 21 \times 37.5 \text{ cm}^3$. A user-friendly interface was also introduced. Basically, the user selects pulse amplitude, number of pulses, pulse frequency, and triggers the generation. Two diodes serve as indicators for ongoing pulsing. All the buttons (except emergency discharge) are blocked by software to prevent any manipulation of the parameters during the burst.

C. HI-PEMF Applicator

As an applicator, solenoid coils are used. In this article, we have tested three different coils of similar inductance (11.8–14 μH) and varied the effective volume (inner radius, r). Enamel-insulated copper wire was used for the windings. The following designs were implemented: Coil 1: ($6L \times 8W$, wire: 0.5 mm, and $r = 2 \text{ mm}$); Coil 2: ($6L \times 8W$, wire: 0.8 mm, and $r = 2 \text{ mm}$); and Coil 3: ($6L \times 8W$, wire: 0.8 mm, and $r = 3 \text{ mm}$), where L and W stand for layers and windings, respectively. The inner diameter of the coils was adjusted to match the tip of the standard 0.2 mL sterile PCR tube (ABgene, ThermoFisher Scientific, Portsmouth, NH, USA), where the cells were placed for the treatment.

The photographs of the coils and the resultant pulse shapes are shown in Fig. 3. The MF was measured by a calibrated B-dot sensor (VGTU, Vilnius, Lithuania). The peak current value was estimated on a series shunt resistance R_{shunt} (see Fig. 1). Since the resultant inductances of the coils are comparable, the currents are also similar (0.92–1 kA), but the physical dimensions of the coils vary, therefore, the MF pulse amplitudes differ significantly. As shown in Fig. 3(b), the highest MF value (6.7 T, 3 kV charging voltage) is achieved using the Coil 1, followed by Coils 2 and 3.

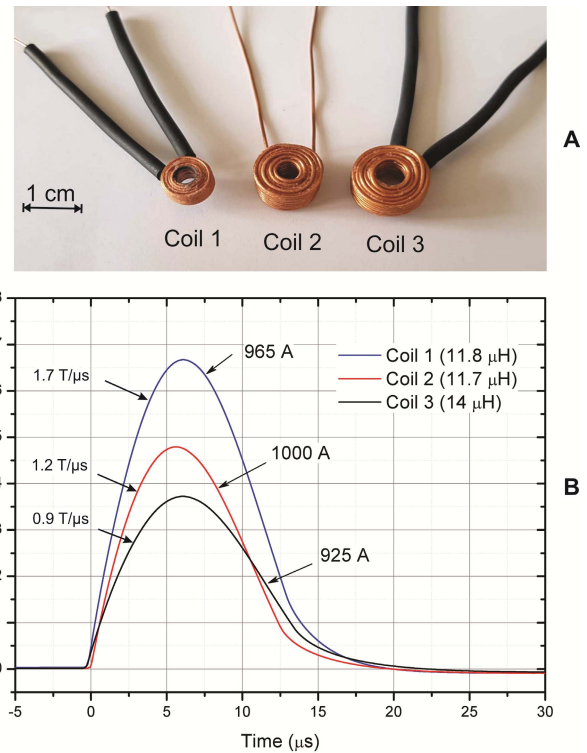


Fig. 3. Photograph of the (a) developed applicators and (b) resultant MF pulses. Acquired using Tektronix DPO4034, post-processed in OriginLab 8.5.

D. Joule Heating

Taken that the current is considerably higher compared to the previous implementations of generators (1 kA + versus 0.55 kA [50]), we have used ice cooling of the coils. The temperature rise was measured by the fiber optic sensor system (opSens, Québec, QC, Canada), which consisted of ProSens signal conditioner and a fiber optic temperature sensor OTG-M170. The sensor has been placed inside the PCR tube filled with phosphate buffered saline (PBS), and a burst of 100 pulses (1 Hz) of maximum amplitude has been delivered.

As shown in Fig. 4(a), without cooling the temperature rise is considerable and already after 60 pulses, the temperature exceeds 40 °C for Coil 1. Ice cooling allowed to improve the situation and stabilize the temperature. In the case of Coil 3, due to the largest volume and thus heat dissipation, the temperature of the sample was stabilized at 15 °C during constant pulsing. Nevertheless, cooling with ice involves some deviation in temperature between different sessions, which is mainly due to the varied (random) area of contact of ice cubes and the coil. Therefore, we have performed several independent measurements of “hottest” Coil 1 to account for the effect. The results are presented in Fig. 4(b). The repositioning/steering of ice (due to melting) has an effect on the cooling efficiency; however, the deviation is within $\pm 3 \text{ }^\circ\text{C}$.

E. Distribution of Magnetic and Electric Fields

As mentioned above, the induced electric field $> 5 \text{ V/cm}$ seems to be crucial for the successful contactless permeabilization of mammalian cells. However, it is known that in solenoid-type inductors the induced electric field is

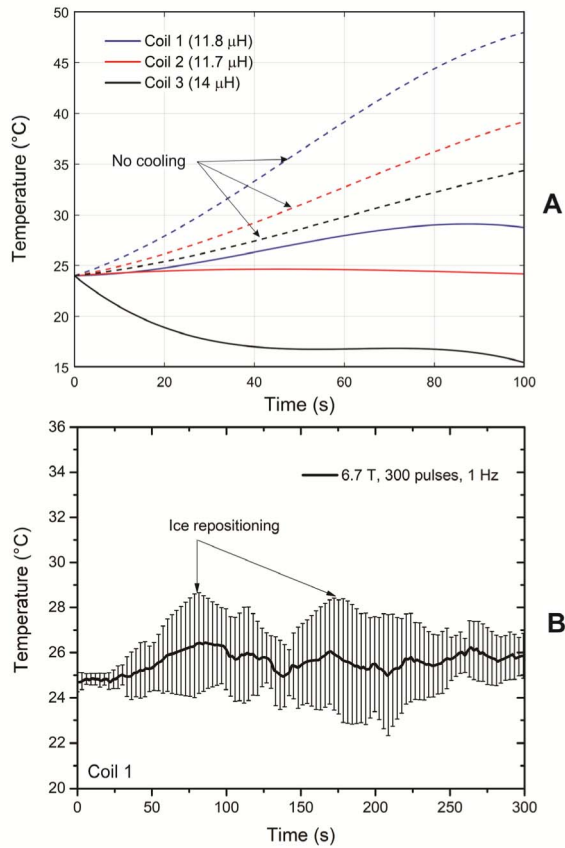


Fig. 4. (a) Temperature rise due to pulse delivery with (solid lines) and without (dashed lines) ice cooling. (b) Deviation of temperature rise is apparent between independent sessions, where the solid line represents average temperature rise and the time of ice repositioning is marked.

non-homogeneous and is linearly decreasing to 0 (center of the coil) [59]. The resultant MF distribution and electric field distribution were estimated using COMSOL Multiphysics 5.4 (COMSOL, Stockholm, Sweden).

A 2-D axisymmetric model of the inductors has been designed using the MFs physics module. As an input, the measured current pulse waveform was used and an automated physics-controlled meshing was applied. The simulated MF amplitude for Coil 1 is shown in Fig. 5(a). The peak value in the center of the coil is in good agreement ($\pm 5\%$) with the experimental pulse that is presented in Fig. 3. According to the model, the homogeneity of the distribution is acceptable, and the variance does not exceed $\pm 15\%$ of the amplitude in the center.

The spatial distribution of the electric field was then estimated and presented in Fig. 5(b). The peak value of 15–17 V/cm was estimated near the coil windings. The waveform of the induced electric field for Coil 1 during the highest dB/dt of the pulse in comparison to other coils is shown in Fig. 6.

It can be seen that Coil 1 due to the highest dB/dt ratio allows generating induced electric >15 V/cm, which is in agreement with the target parameters. Taking into account the PEF and pulsed magnetic field (PMF) amplitudes and the well-controlled Joule heating, the study was further limited to the superior Coil 1.

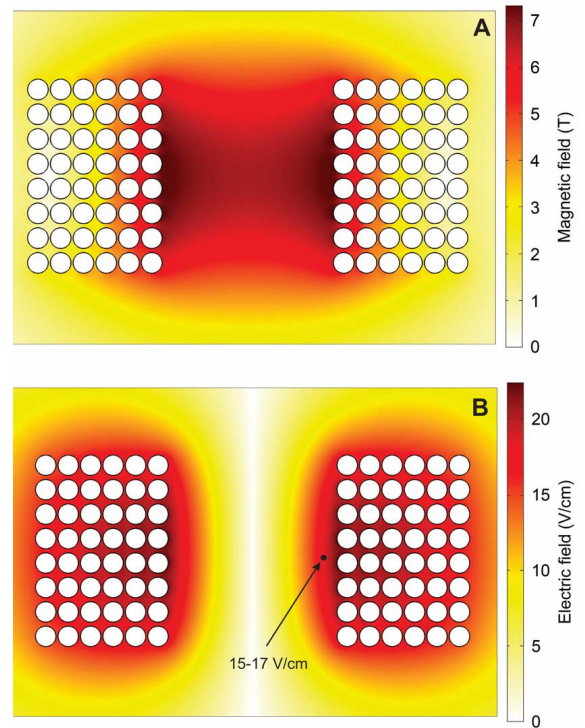


Fig. 5. Spatial distributions of (a) MF and (b) electric field. Electric field was estimated during the highest dB/dt of the pulse.

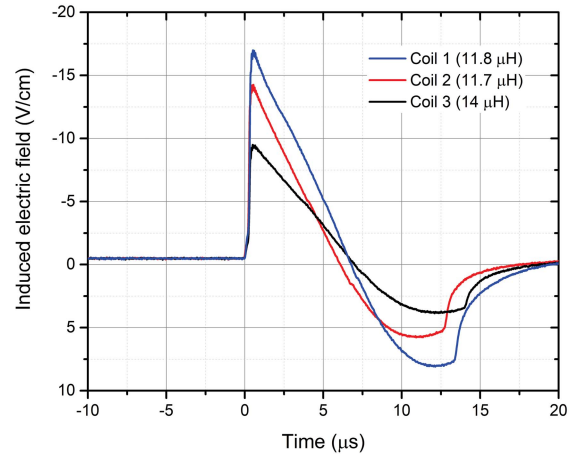


Fig. 6. Induced electric field near coil windings during the highest dB/dt of each inductor.

III. EXPERIMENTAL DATA

A. Cell Preparation

Chinese Hamster Ovary (CHO) cells (European Collection of Authenticated Cell Cultures ECACC, cells CHO-K1, cat. no. 85051005, obtained directly from the repository) were grown in 25 cm² culture flasks (TPP, Trasadingen, Switzerland) in HAM F-12 growth medium (PAA Laboratories GmbH, Pasching, Austria) for 2–3 days in an incubator (Kambič, Semič, Slovenia) at 37 °C and humidified 5% CO₂. The growth medium (used in this composition through all experiments) was supplemented with 10% fetal bovine serum (Sigma-Aldrich, Schnellendorf, Germany), L-glutamine (StemCell, Vancouver, BC, Canada), and antibiotics penicillin/streptomycin (PAA, Austria), and gentamycin (Sigma-Aldrich, Germany). The cell suspension was prepared on the

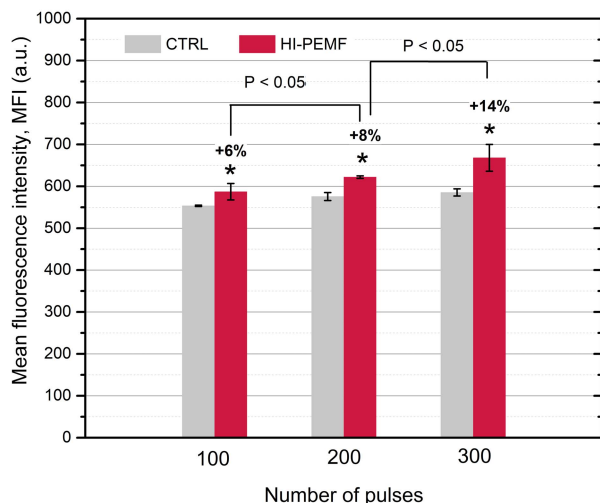


Fig. 7. Permeabilization of CHO cell using HI-PEMF, where CTRL, untreated control, which was incubated at 37 °C, humidified 5% CO₂ for the whole treatment time and HI-PEMF treated samples.

day of carrying out the experiments. Cells were detached by 10× trypsin-EDTA (PAA, Austria), diluted 1:9 in Hank's basal salt solution (StemCell, Canada), and the trypsin was inactivated by the HAM F-12 growth medium. Cells were transferred to a 50 mL centrifuge tube (TPP, Trasadingen, Switzerland) and centrifuged 5 min at 180g and 22 °C. The supernatant was removed, and cells were resuspended in the growth medium HAM F-12 at cell density 10⁷ cells/mL.

B. Permeabilization Assay

The cell suspension was mixed with propidium iodide (PI) at its final concentration of 136 μM. A 40 μL of the cells-dye mixture was transferred into a 0.2 mL PCR tube, followed by HI-PEMF treatment. Three minutes after the last pulse, the cell suspension was mixed with phosphate-potassium buffer (10 mM KH₂PO₄/K₂HPO₄, 1 mM MgCl₂, and 250 mM sucrose) and transferred to a 5 mL tube (Sarsted, Germany) for further analysis using flow cytometry (Life Technologies, Attune NxT, Carlsbad, CA, USA). Cells were excited with a blue laser at 488 nm, and the emitted fluorescence was detected through a 574 nm/26 nm bandpass filter (PI). Fluorescence was determined as the mean value of the gated cells of the measured signal [mean fluorescence intensity (MFI)]. The gate was defined based on untreated control. The experiments were performed in triplicates in random order.

The generator was tested at a maximum amplitude with Coil 1 (6.7 T, 17 V/cm) and bursts of 100, 200, and 300 pulses were delivered at a repetition frequency of 1 Hz. The results are summarized in Fig. 7.

As can be seen, 6.7 T, 17 V/cm pulses trigger the uptake of PI by the cells. A tendency of the efficiency to scale with an increase in the number of pulses was observed.

IV. CONCLUSION

We developed a compact HI-PEMF generator, which is capable of handling currents up to 1.5 kA and supporting inductive loads >5 μH. It was successfully tested in basic

cell membrane permeabilization experiments. We have shown that 6.7 T, 17 V/cm microsecond range pulses are sufficient to trigger contactless permeabilization *in vitro*. Taking into account the non-homogeneity of the PEF during HI-PEMF, future setups should focus on the development of new applicators, which would allow ensuring higher fields and uniform exposure of the cells. One of the possible solutions is the implementation of a physical barrier inside the cuvette, which would keep the cells in the high electric field region. The proposed power electronics circuit and robust implementation is universal and does not depend on the geometry of the exposure tube.

ACKNOWLEDGMENT

This work was supported in part by the Research Council of Lithuania under Grant S-MIP-19-13 and in part by the Slovenian Research Agency through research core funding under Grant P2-0249 and Grant J2-9225 to DM. Experiments were performed within the Infrastructure Programme: Network of research infrastructure centers at the University of Ljubljana (MRIC UL IP-0510).

REFERENCES

- [1] T. Y. Y. Tsong, "Electroporation of cell membranes," *Biophys. J.*, vol. 60, no. 2, pp. 297–306, 1991.
- [2] T. Kotnik, P. Kramar, G. Pucihar, D. Miklavcic, and M. Tarek, "Cell membrane electroporation—Part 1: The phenomenon," *IEEE Elect. Insul. Mag.*, vol. 28, no. 5, pp. 14–23, Sep. 2012.
- [3] T. Kotnik, L. Rems, M. Tarek, and D. Miklavcic, "Membrane electroporation and electroporation: Mechanisms and models," *Annu. Rev. Biophys.*, vol. 48, no. 1, pp. 63–91, May 2019.
- [4] P. Sánchez-Velázquez *et al.*, "Irreversible electroporation of the liver: Is there a safe limit to the ablation volume?" *Sci. Rep.*, vol. 6, Apr. 2016, Art. no. 23781.
- [5] M. B. Sano, O. Volotskova, and L. Xing, "Treatment of cancer in vitro using radiation and high-frequency bursts of submicrosecond electrical pulses," *IEEE Trans. Biomed. Eng.*, vol. 65, no. 4, pp. 928–935, Apr. 2018.
- [6] T. Garcia-Sanchez *et al.*, "Successful tumor electrochemotherapy using sine waves," *IEEE Trans. Biomed. Eng.*, to be published.
- [7] A. Golberg *et al.*, "Energy-efficient biomass processing with pulsed electric fields for bioeconomy and sustainable development," *Biotechnol. Biofuels*, vol. 9, no. 1, p. 94, Dec. 2016.
- [8] T. Kotnik, W. Frey, M. Sack, S. H. Meglič, M. Peterka, and D. Miklavcic, "Electroporation-based applications in biotechnology," *Trends Biotechnol.*, vol. 33, no. 8, pp. 480–488, Aug. 2015.
- [9] V. Mutsenko *et al.*, "Me₂SO- and serum-free cryopreservation of human umbilical cord mesenchymal stem cells using electroporation-assisted delivery of sugars," *Cryobiology*, vol. 91, pp. 104–114, Dec. 2019.
- [10] M. Rebersek, D. Miklavcic, C. Bertacchini, and M. Sack, "Cell membrane electroporation—Part 3: The equipment," *IEEE Elect. Insul. Mag.*, vol. 30, no. 3, pp. 8–18, May 2014.
- [11] A. E. Rubin, K. Levkov, O. B. Usta, M. Yarmush, and A. Golberg, "IGBT-based pulsed electric fields generator for disinfection: Design and in vitro studies on *Pseudomonas aeruginosa*," *Ann. Biomed. Eng.*, vol. 47, no. 5, pp. 1314–1325, May 2019.
- [12] V. Novickij *et al.*, "High-frequency submicrosecond electroporator," *Biotechnol. Biotechnol. Equip.*, vol. 30, no. 3, pp. 607–613, May 2016.
- [13] J. Zhao *et al.*, "Irreversible electroporation reverses resistance to immune checkpoint blockade in pancreatic cancer," *Nature Commun.*, vol. 10, no. 1, Dec. 2019, Art. no. 899.
- [14] M. B. Sano *et al.*, "Reduction of muscle contractions during irreversible electroporation therapy using high-frequency bursts of alternating polarity pulses: A laboratory investigation in an ex vivo swine model," *J. Vascular Interventional Radiol.*, vol. 29, no. 6, pp. 893.e4–898.e4, Jun. 2018.
- [15] E. L. Latouche *et al.*, "High-frequency irreversible electroporation for intracranial meningioma: A feasibility study in a spontaneous canine tumor model," *Technol. Cancer Res. Treatment*, vol. 17, Jan. 2018, Art. no. 153303381878528.

- [16] D. Zhao, M. Wu, D. Huang, Z. Liang, Z. Wei, and Z. Li, "Parametric optimization of electric field strength for cancer electrochemotherapy on a chip-based model," *Theranostics*, vol. 8, no. 2, pp. 358–368, 2018.
- [17] S. Romeo *et al.*, "ESOPe-equivalent pulsing protocols for calcium electroporation: An in vitro optimization study on 2 cancer cell models," *Technol. Cancer Res. Treatment*, vol. 17, Jan. 2018, Art. no. 153303381878807.
- [18] P. A. Garcia, J. H. Rossmeis, R. E. Neal, T. L. Ellis, and R. V. Davalos, "A parametric study delineating irreversible electroporation from thermal damage based on a minimally invasive intracranial procedure," *Biomed. Eng. OnLine*, vol. 10, no. 1, Dec. 2011.
- [19] Y. Mi *et al.*, "Multi-parametric study of temperature and thermal damage of tumor exposed to high-frequency nanosecond-pulsed electric fields based on finite element simulation," *Med. Biol. Eng. Comput.*, vol. 55, no. 7, pp. 1109–1122, Jul. 2017.
- [20] Z. A. Steelman, G. P. Tolstykh, H. T. Beier, and B. L. Ibey, "Cellular response to high pulse repetition rate nanosecond pulses varies with fluorescent marker identity," *Biochem. Biophys. Res. Commun.*, vol. 478, no. 3, pp. 1261–1267, Sep. 2016.
- [21] R. C. G. Martin *et al.*, "Irreversible electroporation in locally advanced pancreatic cancer: A call for standardization of energy delivery," *J. Surgical Oncol.*, vol. 114, no. 7, pp. 865–871, Dec. 2016.
- [22] M. Cemazar, G. Sersa, W. Frey, D. Miklavčič, and J. Teissié, "Recommendations and requirements for reporting on applications of electric pulse delivery for electroporation of biological samples," *Bioelectrochemistry*, vol. 122, pp. 69–76, Aug. 2018.
- [23] W. van den Bos *et al.*, "The correlation between the electrode configuration and histopathology of irreversible electroporation ablations in prostate cancer patients," *World J. Urol.*, vol. 34, no. 5, pp. 657–664, May 2016.
- [24] R. E. Neal, R. Singh, H. C. Hatcher, N. D. Kock, S. V. Torti, and R. V. Davalos, "Treatment of breast cancer through the application of irreversible electroporation using a novel minimally invasive single needle electrode," *Breast Cancer Res. Treat.*, vol. 123, no. 1, pp. 295–301, Aug. 2010.
- [25] F. Mahmood and J. Gehl, "Optimizing clinical performance and geometrical robustness of a new electrode device for intracranial tumor electroporation," *Bioelectrochemistry*, vol. 81, no. 1, pp. 10–16, Apr. 2011.
- [26] L. G. Campana *et al.*, "Electrochemotherapy—Emerging applications technical advances, new indications, combined approaches, and multi-institutional collaboration," *Eur. J. Surgical Oncol.*, vol. 45, no. 2, pp. 92–102, Feb. 2019.
- [27] J. F. Edd and R. V. Davalos, "Mathematical modeling of irreversible electroporation for treatment planning," *Technol. Cancer Res. Treat.*, vol. 6, no. 4, pp. 275–286, Aug. 2007.
- [28] A. Zupanic, B. Kos, and D. Miklavčič, "Treatment planning of electroporation-based medical interventions: Electrochemotherapy, gene electrotransfer and irreversible electroporation," *Phys. Med. Biol.*, vol. 57, no. 17, pp. 5425–5440, Sep. 2012.
- [29] A. Golberg, B. G. Bruinsma, B. E. Uygun, and M. L. Yarmush, "Tissue heterogeneity in structure and conductivity contribute to cell survival during irreversible electroporation ablation by 'electric field sinks,'" *Sci. Rep.*, vol. 5, no. 1, Jul. 2015, Art. no. 8485.
- [30] L. G. Campana *et al.*, "Effect of tissue inhomogeneity in soft tissue sarcomas: From real cases to numerical and experimental models," *Technol. Cancer Res. Treat.*, vol. 17, Jan. 2018, Art. no. 153303381878969.
- [31] J. Langus, M. Kranjc, B. Kos, T. Šuštar, and D. Miklavčič, "Dynamic finite-element model for efficient modelling of electric currents in electroporated tissue," *Sci. Rep.*, vol. 6, no. 1, Sep. 2016, Art. no. 26409.
- [32] Y. Mi *et al.*, "Scaling relationship of *in vivo* muscle contraction strength of rabbits exposed to high-frequency nanosecond pulse bursts," *Technol. Cancer Res. Treatment*, vol. 17, Jan. 2018, Art. no. 153303381878807.
- [33] K. Nielsen *et al.*, "Anaesthetic management during open and percutaneous irreversible electroporation," *Brit. J. Anaesthesia*, vol. 113, no. 6, pp. 985–992, Dec. 2014.
- [34] A. Deodhar *et al.*, "Irreversible electroporation near the heart: Ventricular arrhythmias can be prevented with ECG synchronization," *Amer. J. Roentgenol.*, vol. 196, no. 3, pp. W330–W335, Mar. 2011.
- [35] R. Rodaite-Riseviciene, R. Saule, V. Snitka, and G. Saulis, "Release of iron ions from the stainless steel anode occurring during high-voltage pulses and its consequences for cell electroporation technology," *IEEE Trans. Plasma Sci.*, vol. 42, no. 1, pp. 249–254, Jan. 2014.
- [36] F. Maglietti, S. Michinski, N. Olaiz, M. Castro, C. Suárez, and G. Marshall, "The role of pH fronts in tissue electroporation based treatments," *PLoS ONE*, vol. 8, no. 11, 2013, Art. no. e80167.
- [37] E. Luján, M. Marino, N. Olaiz, and G. Marshall, "Towards an optimal dose-response relationship in gene electrotransfer protocols," *Electrochimica Acta*, vol. 319, pp. 1002–1011, Oct. 2019.
- [38] M. Phillips, H. Krishnan, N. Raju, and B. Rubinsky, "Tissue ablation by a synergistic combination of electroporation and electrolysis delivered by a single pulse," *Ann. Biomed. Eng.*, vol. 44, no. 10, pp. 3144–3154, Oct. 2016.
- [39] N. Klein *et al.*, "The combination of electroporation and electrolysis (E2) employing different electrode arrays for ablation of large tissue volumes," *PLoS ONE*, vol. 14, no. 8, 2019, Art. no. e0221393.
- [40] D. O. H. Suzuki, C. M. G. Marques, and M. M. M. Rangel, "Conductive gel increases the small tumor treatment with electrochemotherapy using needle electrodes," *Artif. Organs*, vol. 40, no. 7, pp. 705–711, 2016.
- [41] C. Yao *et al.*, "Bipolar microsecond pulses and insulated needle electrodes for reducing muscle contractions during irreversible electroporation," *IEEE Trans. Biomed. Eng.*, vol. 64, no. 12, pp. 2924–2937, Dec. 2017.
- [42] E. Guenther, N. Klein, P. Mikus, M. K. Stehling, and B. Rubinsky, "Electrical breakdown in tissue electroporation," *Biochem. Biophys. Res. Commun.*, vol. 467, no. 4, pp. 736–741, Nov. 2015.
- [43] T. J. Kardos and D. P. Rabussay, "Contactless magneto-permeabilization for intracellular plasmid DNA delivery *in-vivo*," *Human Vaccines Immunotherapeutics*, vol. 8, no. 11, pp. 1707–1713, Nov. 2012.
- [44] L. Towhidi, S. Firoozabadi, H. Mozdarani, and D. Miklavcic, "Lucifer yellow uptake by CHO cells exposed to magnetic and electric pulses," *Radiol. Oncol.*, vol. 46, no. 2, pp. 25–119, Jan. 2012.
- [45] S. Kranjc, M. Kranjc, J. Scancar, J. Jelenc, G. Sersa, and D. Miklavcic, "Electrochemotherapy by pulsed electromagnetic field treatment (PEMF) in mouse melanoma B16F10 *in vivo*," *Radiol. Oncol.*, vol. 50, no. 1, pp. 39–48, Mar. 2016.
- [46] V. Novickij *et al.*, "Pulsed electromagnetic field assisted in vitro electroporation: A pilot study," *Sci. Rep.*, vol. 6, no. 1, Dec. 2016, Art. no. 33537.
- [47] S. K. Brezar, M. Kranjc, M. Cemazar, S. Bucek, G. Serša, and D. Miklavčič, "Electrotransfer of siRNA to silence enhanced green fluorescent protein in tumor mediated by a high intensity pulsed electromagnetic field," *Vaccines*, vol. 8, no. 1, p. 49, 2020.
- [48] V. Novickij *et al.*, "Different permeabilization patterns of splenocytes and thymocytes to combination of pulsed electric and magnetic field treatments," *Bioelectrochemistry*, vol. 122, pp. 183–190, Aug. 2018.
- [49] V. Novickij, A. Grainys, I. Kucinskaitė-Kodze, A. Zvirbliene, and J. Novickij, "Magneto-permeabilization of viable cell membrane using high pulsed magnetic field," *IEEE Trans. Magn.*, vol. 51, no. 9, pp. 1–5, Sep. 2015.
- [50] V. Novickij, J. Dermol, A. Grainys, M. Kranjc, and D. Miklavčič, "Membrane permeabilization of mammalian cells using bursts of high magnetic field pulses," *PeerJ*, vol. 5, Apr. 2017, Art. no. e3267.
- [51] V. Novickij, A. Grainys, J. Novickij, and A. Lucinskis, "Programmable pulsed magnetic field system for biological applications," *IEEE Trans. Magn.*, vol. 50, no. 11, pp. 1–4, Nov. 2014.
- [52] V. Novickij, S. Markovskaja, A. Grainys, and J. Novickij, "Irreversible magnetoporation of micro-organisms in high pulsed magnetic fields," *IET Nanobiotechnology*, vol. 8, no. 3, pp. 157–162, Sep. 2014.
- [53] V. Novickij, A. Grainys, J. Švedienė, S. Markovskaja, and J. Novickij, "Joule heating influence on the vitality of fungi in pulsed magnetic fields during magnetic permeabilization," *J. Thermal Anal. Calorimetry*, vol. 118, no. 2, pp. 681–686, Nov. 2014.
- [54] J. W. M. van Bree, J. J. G. Geysen, E. J. M. van Heesch, and A. J. M. Pemen, "Novel nanosecond pulsed electric field device for noncontact treatment of cells in native culture conditions," *IEEE Trans. Plasma Sci.*, vol. 41, no. 10, pp. 2654–2658, Oct. 2013.
- [55] V. Novickij, A. Grainys, J. Novickij, A. Lucinskis, and P. Zapolskis, "Compact microsecond pulsed magnetic field generator for application in bioelectronics," *Electron. Electr. Eng.*, vol. 19, no. 8, pp. 25–28, 2013.
- [56] V. Novickij, A. Grainys, G. Staigvila, S. Tolvaisiene, T. Ustinavicius, and J. Novickij, "Design and optimization of pulsed magnetic field generator for cell magneto-permeabilization," *Elektronika Elektrotechnika*, vol. 23, no. 2, pp. 21–25, 2017.
- [57] H. Xiong, W. Sun, J. Liu, and J. Shi, "A multifunctional energy-saving magnetic field generator," *Rev. Sci. Instrum.*, vol. 89, no. 3, Mar. 2018, Art. no. 034704.
- [58] G. Staigvila, V. Novickij, and J. Novickij, "Fast ignitron-based magnetic field pulser for biological applications," *IEEE Trans. Magn.*, vol. 55, no. 5, May 2019, Art. no. 5900105.
- [59] V. Novickij *et al.*, "Reversible permeabilization of cancer cells by high sub-microsecond magnetic field," *IEEE Trans. Magn.*, vol. 53, no. 11, Nov. 2017, Art. no. 2001904.